Improved study of the β-function of $SU(3)$ gauge theory with $N_f = 10$ massless domain-wall fermions

Ting-Wai Chiu

Physics Department, National Taiwan Normal University, Taipei, Taiwan 11677, Republic of China;
Institute of Physics, Academia Sinica, Taipei, Taiwan 11529, Republic of China;
and Physics Department, National Taiwan University, Taipei, Taiwan 10617, Republic of China

We perform an improved study of the β function of $SU(3)$ lattice gauge theory with $N_f = 10$ massless optimal domain-wall fermions in the fundamental representation, which serves as a check to what extent the scenario we presented previously [*Proc. Sci.*, LATTICE2016 (2017) 228] is valid. In the finite-volume gradient flow scheme with $c = \sqrt{8t}/L = 0.3$, the renormalized couplings $g^2(L, a)$ of four primary lattices ($L/a = \{8, 10, 12, 16\}$) are tuned (in $6/g_0^2$) to the same g_c^2 with statistical error less than 0.5%, in contrast to the previous work where $g^2(L, a)$ were obtained by the cubic-spline interpolation. Then, the renormalized couplings $g^2(sL, a)$ of the scaled lattices ($sL/a = \{16, 20, 24, 32\}$ with $s = 2$) are computed at the same $6/g_0^2$ of the corresponding primary lattices. Using the renormalized couplings of four lattice pairs $(sL, L)/a = \{(16, 8), (20, 10), (24, 12), (32, 16)\}$, the step-scaling β function $[g^2(sL, a) - g^2(L, a)]/\ln(s^2)$ is computed and extrapolated to the continuum limit $\beta(s, g_c^2)$, as summarized in Table III. Based on the four data points of $\beta(s, g_c^2)$ at $g_c^2 = \{6.86(2), 6.92(3), 7.03(2), 7.16(2)\}$, we infer that the theory is infrared near-conformal, or conformal with the fixed point $g_*^2 = 7.55(36)$. This corrects the scenario in the previous work with $g_*^2 \sim 7.0$, and also suggests that the interpolation method cannot give a reliable determination of the β function, especially in a regime close to the infrared fixed point.

I. INTRODUCTION

In Refs. [1,2], we investigated the β function of the $SU(3)$ gauge theory with $N_f = 10$ massless optimal domain-wall fermions in the fundamental representation. The motivation was to see whether this theory possesses a nontrivial infrared fixed point, which is not only a fundamental problem in quantum field theory, but also relevant to beyond the Standard Model scenarios with a composite Higgs boson. (For recent reviews, see, e.g., Refs. [3–5].) The results in Refs. [1,2] suggest that the theory might possess an infrared fixed point (IRFP) around $g_c^2 \sim 7$. However, the major systematic uncertainty in Refs. [1,2] was that interpolation was used to obtain the renormalized couplings $g^2(L, a)$ and $g^2(sL, a)$. This could lead to a large systematic error in the strong-coupling regime where the renormalized coupling varies rapidly with respect to the bare coupling g_0 (or $6/g_0^2$), which in turn may give incorrect results for the step-scaling β function

$$\beta(s, a/L, g^2) = \frac{g^2(sL, a) - g^2(L, a)}{\ln(s^2)}, \qquad (1)$$

as well as its extrapolated value in the continuum limit ($a/L \rightarrow 0$). The purpose of the present study is to eliminate this systematic uncertainty by tuning $6/g_0^2$ such that the renormalized couplings $g^2(L, a)$ of all primary lattices ($L/a = 8, 10, 12, 16$) have the same value with a statistical error less than 0.5%. The tuning process implies that many simulations on the primary lattices have to be performed, which are rather challenging in terms of computing resources, time, and effort. After the value of $6/g_0^2$ is determined for a chosen $g_c^2 = g^2(L, a)$, the simulation on the scaled ($s = 2$) lattice is performed at the same $6/g_0^2$ to obtain the renormalized coupling $g^2(sL, a)$. Since the results in Refs. [1,2] suggest that the theory may possess an infrared fixed point around $g_c^2 \sim 7$, four targeted values of $g_c^2 = \{6.86(2), 6.92(3), 7.03(2), 7.16(2)\}$ around $g_c^2 = 7.0$ are chosen. Also, a point at $g_c^2 = 3.51(2)$ is picked to check whether the interpolation used in Refs. [1,2] works well in the regime where the renormalized coupling varies slowly with respect to the bare coupling. Moreover, in view of a recent study of the $SU(3)$ gauge theory with $N_f = 10$ massless domain-wall fermions [6] (which reported 2–3 standard deviations compared with the results of Ref. [2] for $4.5 < g_c^2 < 6.0$), a point at $g_c^2 = 5.25(2)$ is chosen to

check whether the discrepancy is due to the systematic error of the interpolation used in Ref. [2]. All together, the targeted values of g_c^2 in this study are $g_c^2 = \{3.51(2), 5.25(2), 6.86(2), 6.92(3), 7.03(2), 7.16(2)\}$.

The outline of this paper is as follows. In Sec. II, we describe our hybrid Monte Carlo (HMC) simulation of $SU(3)$ gauge theory with $N_f = 10$ massless optimal domain-wall fermions, and summarize the residual masses of all gauge ensembles in Table I. In Sec. III, we present our results for the renormalized couplings in the finite-volume gradient flow scheme with $c = \sqrt{8t}/L = 0.3$, for all gauge ensembles, as summarized in Table II. In Sec. IV, we perform the extrapolation of the step-scaling β function $\beta(s, a/L, g_c^2)$ to the continuum limit ($a/L \to 0$) with the linear fit $[A + B(a/L)^2]$ and quadratic fit $[A + B(a/L)^2 + C(a/L)^4]$. The results are summarized in Table III. In Sec. V, we perform the extrapolation of $\beta(s, g_c^2)$ with the linear fit using four data points at $g_c^2 = \{6.86(2), 6.92(3), 7.03(2), 7.16(2)\}$, and determine the IRFP g_*^2 and the slope of $\beta(s, g^2)$ at the IRFP. In Sec. VI, we determine the universal scaling exponent γ_g^* of the conventional β function $\beta(g^2(\mu))$ in the continuum, with the input of the slope of $\beta(s, g^2)$ at the IRFP. In Sec. VII, we summarize the results of this paper, and discuss the discrepancies

TABLE I. The residual masses of all gauge ensembles in this work.

$6/g_0^2$	L/a	$(m_{\rm res}a)_L$	$2L/a$	$(m_{\rm res}a)_{2L}$
6.4650	16	$5.8(3) \times 10^{-5}$	32	$5.4(2) \times 10^{-5}$
6.4730	16	$5.3(1) \times 10^{-5}$	32	$4.9(7) \times 10^{-5}$
6.4750	16	$5.7(4) \times 10^{-5}$	32	$5.6(5) \times 10^{-5}$
6.4800	16	$5.2(8) \times 10^{-5}$	32	$5.2(2) \times 10^{-5}$
6.6000	16	$4.6(1) \times 10^{-5}$	32	$4.5(3) \times 10^{-5}$
7.0000	16	$4.5(6) \times 10^{-5}$	32	$4.4(1) \times 10^{-5}$
6.4610	12	$5.9(3) \times 10^{-5}$	24	$6.3(5) \times 10^{-5}$
6.4645	12	$5.8(2) \times 10^{-5}$	24	$6.2(4) \times 10^{-5}$
6.4680	12	$6.2(6) \times 10^{-5}$	24	$5.5(2) \times 10^{-5}$
6.4690	12	$5.5(3) \times 10^{-5}$	24	$5.9(6) \times 10^{-5}$
6.5700	12	$4.9(3) \times 10^{-5}$	24	$4.5(2) \times 10^{-5}$
6.9500	12	$4.5(7) \times 10^{-5}$	24	$4.5(1) \times 10^{-5}$
6.4590	10	$5.8(1) \times 10^{-5}$	20	$7.4(9) \times 10^{-5}$
6.4600	10	$6.6(5) \times 10^{-5}$	20	$6.0(3) \times 10^{-5}$
6.4640	10	$6.5(6) \times 10^{-5}$	20	$5.6(2) \times 10^{-5}$
6.4660	10	$6.4(3) \times 10^{-5}$	20	$5.7(2) \times 10^{-5}$
6.5500	10	$4.8(6) \times 10^{-5}$	20	$4.6(1) \times 10^{-5}$
6.9000	10	$4.6(6) \times 10^{-5}$	20	$4.5(0) \times 10^{-5}$
6.4490	8	$6.2(3) \times 10^{-5}$	16	$8.5(7) \times 10^{-5}$
6.4510	8	$6.1(4) \times 10^{-5}$	16	$7.7(1) \times 10^{-5}$
6.4520	8	$5.9(3) \times 10^{-5}$	16	$6.9(4) \times 10^{-5}$
6.4530	8	$6.0(2) \times 10^{-5}$	16	$6.1(4) \times 10^{-5}$
6.5200	8	$5.1(2) \times 10^{-5}$	16	$4.7(4) \times 10^{-5}$
6.8000	8	$4.7(6) \times 10^{-5}$	16	$4.5(7) \times 10^{-5}$

TABLE II. Summary of the renormalized couplings for all gauge ensembles in this work.

$6/g_0^2$	L/a	$g^2(L, a)$	$2L/a$	$g^2(2L, a)$
6.4650	16	7.16(2)	32	7.68(3)
6.4610	12	7.16(3)	24	7.81(3)
6.4590	10	7.16(2)	20	7.97(4)
6.4490	8	7.15(3)	16	8.02(4)
6.4730	16	7.03(2)	32	7.53(3)
6.4645	12	7.02(3)	24	7.60(3)
6.4600	10	7.03(3)	20	7.67(3)
6.4510	8	7.03(3)	16	7.80(2)
6.4750	16	6.92(3)	32	7.50(3)
6.4680	12	6.93(3)	24	7.56(3)
6.4640	10	6.93(3)	20	7.63(3)
6.4520	8	6.93(3)	16	7.78(3)
6.4800	16	6.86(2)	32	7.48(3)
6.4690	12	6.86(3)	24	7.52(4)
6.4660	10	6.86(3)	20	7.61(4)
6.4530	8	6.86(3)	16	7.76(2)
6.6000	16	5.25(2)	32	5.76(3)
6.5700	12	5.25(3)	24	5.82(3)
6.5500	10	5.26(2)	20	5.88(3)
6.5200	8	5.25(3)	16	5.95(3)
7.0000	16	3.51(2)	32	3.91(3)
6.9500	12	3.50(3)	24	3.97(3)
6.9000	10	3.51(3)	20	4.01(3)
6.8000	8	3.51(2)	16	4.14(2)

TABLE III. Extrapolation of $\beta(s, a/L, g_c^2)$ to the continuum limit.

	Linear fit		Quadratic fit	
g_c^2	$\beta(s, g_c^2)$	χ^2/d.o.f.	$\beta(s, g_c^2)$	χ^2/d.o.f.
7.16(2)	0.239(47)	0.285	0.171(80)	0.773
7.03(2)	0.299(35)	0.140	0.294(87)	0.184
6.92(3)	0.344(36)	0.333	0.381(87)	0.077
6.86(2)	0.371(32)	0.418	0.409(83)	0.318
5.25(2)	0.318(45)	0.104	0.307(75)	0.040
3.51(2)	0.234(30)	0.361	0.249(77)	0.460

between the results in this paper and those obtained with $N_f = 10$ massless staggered fermions in a recent study [7].

II. GENERATION OF THE GAUGE ENSEMBLES

Since we are dealing with massless fermions, it is vital to use lattice fermions with exact chiral symmetry at finite lattice spacing (i.e., domain-wall [8]/overlap [9] fermions) with exactly the same flavor symmetry as their counterpart in the continuum. Theoretically, the effective four-dimensional lattice Dirac operator of the domain-wall fermion with infinite extent in the fifth dimension ($N_s = \infty$) is exactly equal to the overlap Dirac operator,

$$D(m_q) = m_q + \frac{(1 - rm_q)}{2r}[1 + \gamma_5 H(H^2)^{-1/2}],$$

where m_q is the bare fermion mass,

$$r = \frac{1}{2m_0(1 - dm_0)}, \qquad m_0 \in (0, 2),$$

$$H = c\gamma_5 D_w(1 + dD_w)^{-1},$$

D_w is the standard Wilson-Dirac operator minus m_0, and c and d are parameters depending on the variant of the domain-wall fermions. In this study, we set $c = 1$ and $d = 0$, and thus $H = \gamma_5 D_w = H_w$. In practice, the sign function $S(H) \equiv H(H^2)^{-1/2}$ cannot be computed exactly, since H is a very large matrix and it is prohibitively expensive to diagonalize H. The best way to proceed is to use the Zolotarev optimal rational approximation of the sign function $S(H)$. However, HMC [10] simulations on the four-dimensional lattice with the overlap Dirac operator in the Zolotarev approximation encounter enormous difficulties (see, e.g., Refs. [11,12]). On the other hand, for domain-wall fermions (DWFs) with finite N_s in the fifth dimension, HMC simulations can be performed without serious difficulties. However, DWFs could severely break the exact chiral symmetry, depending on the approximate sign function $S(H)$ in the four-dimensional effective Dirac operator.

The chiral symmetry can be maximally preserved on a lattice with finite N_s by optimal domain-wall fermions [13], with the effective four-dimensional lattice Dirac operator exactly equal to the Zolotarev optimal rational approximation of the overlap Dirac operator. In this paper, we use optimal DWFs with the R_5 symmetry [14], whose effective four-dimensional lattice Dirac operator is exactly equal to the "shifted" Zolotarev optimal rational approximation of the overlap operator, with the approximate sign function $S(H)$ satisfying the bound $0 \leq 1 - S(\lambda) \leq 2d_Z$ for $\lambda^2 \in [\lambda_{min}^2, \lambda_{max}^2]$, where d_Z is the maximum deviation $|1 - \sqrt{x}R_Z(x)|_{max}$ of the Zolotarev optimal rational polynomial $R_Z(x)$ of $1/\sqrt{x}$ for $x \in [1, \lambda_{max}^2/\lambda_{min}^2]$, with degrees $(n - 1, n)$ for $N_s = 2n$.

The action of one-flavor optimal DWFs can be written as

$$\begin{aligned}S(\bar{\Psi}, \Psi, U) = \bar{\Psi}_{x,s}[(\omega_s D_w + 1)_{xx'}\delta_{ss'} \\ + (\omega_s D_w - 1)_{xx'}L_{ss'}]\Psi_{x',s'},\end{aligned} \quad (2)$$

where the indices x and x' denote the sites on the four-dimensional spacetime lattice, s and s' are the indices in the fifth dimension, and the lattice spacing a and the Dirac and color indices have been suppressed. Here D_w is the standard Wilson-Dirac operator minus the parameter $m_0 \in (0, 2)$. The operator L is independent of the gauge field, and it can be written as

$$L = P_+L_+ + P_-L_-, \qquad P_\pm = (1 \pm \gamma_5)/2,$$

and

$$(L_+)_{ss'} = (L_-)_{s's} = \begin{cases} -m_q/(2m_0)\delta_{N_s,s'}, & s = 1, \\ \delta_{s-1,s'}, & 1 < s \leq N_s, \end{cases} \quad (3)$$

where m_q is the bare fermion mass, $m_0 \in (0, 2)$, and N_s is the number of sites in the fifth dimension. For massless DWFs, m_q is set to zero. Besides Eq. (2), the action for the Pauli-Villars fields with $m_q = 2m_0$ has to be included for the cancellation of the bulk modes, which is exactly the same as Eq. (2) except for $m_q = 2m_0$ in $L_\pm$ [Eq. (3)]. Thus the action for $SU(3)$ lattice gauge theory with $N_f = 10$ massless optimal DWFs can be written as

$$S_g(U) + \sum_{f=1}^{10} \{S_{m_q=0}(\bar{\Psi}, \Psi, U)_f + S_{m_q=2m_0}^{PV}(\bar{\Phi}, \Phi, U)_f\},$$

where $S_g(U)$ is the gauge action. In this paper, we use the Wilson plaquette gauge action

$$S_g(U) = \frac{6}{g_0^2} \sum_{plaq} \left\{1 - \frac{1}{3}\text{ReTr}(U_p)\right\},$$

where g_0 is the bare coupling. For the fermion action, we set $m_0 = 1.8$ and $N_s = 16$. The optimal weights ω_s [14] are computed with $\lambda_{max}/\lambda_{min} = 6.2/0.05$.

Simulating $N_f = 10$ DWFs amounts to simulating five pairs of $N_f = 2$ DWFs. Starting from the action (2) and following the procedures of even-odd preconditioning and the Schur decomposition given in Ref. [15], the partition function for the $SU(3)$ gauge theory with $N_f = 10$ massless optimal DWFs can be written as

$$\begin{aligned}Z = \int [dU] \prod_{i=1}^{5} [d\phi^\dagger]_i[d\phi]_i \\ \times \exp\left(-S_g[U] - \sum_{i=1}^{5} \phi_i^\dagger(C_{PV}^\dagger)_i(CC^\dagger)_i^{-1}(C_{PV})_i\phi_i\right),\end{aligned} \quad (4)$$

where ϕ_i and $\phi_i^\dagger$ are pseudofermion fields, and

$$C = 1 - M_5 D_w^{OE} M_5 D_w^{EO},$$

$$M_5 = \{(4 - m_0) + \omega_s^{-1/2}[(1 - L)(1 + L)^{-1}]_{s,s'}\omega_{s'}^{-1/2}\}^{-1}.$$

However, HMC simulations with Eq. (4) turn out to be rather time consuming for large lattices at strong couplings, e.g., 32^4 at $6/g_0^2 = 6.45$. To resolve this difficulty, we use a

novel $N_f = 2$ pseudofermion action based on the exact pseudofermion action for one-flavor DWFs [16], which turns out to be more efficient than (4). This novel $N_f = 2$ pseudofermion action for optimal DWFs can be written as $S = \Phi^\dagger K(m)^\dagger K(m) \Phi$, where

$$K(m) = 1 + \left(\frac{1-m}{1+m}\right) \gamma_5 v^T \omega^{-1/2} \frac{1}{H_T(m)} \omega^{-1/2} v,$$

$$m = \frac{m_q}{2m_0}, \qquad v = \begin{pmatrix} v_+ & 0 \\ 0 & v_- \end{pmatrix}_{\text{Dirac}}.$$

Here $\omega = \text{diag}(\omega_1, \omega_2 \cdots, \omega_{N_s})$, $v_+ = \text{diag}(-1, 1, \ldots, (-1)^{N_s})$, $v_- = -v_+$, $H_T(m) = R_5 \gamma_5 D_T(m)$, and

$$D_T(m) = D_w + \omega^{-1/2}(1 - L)(1 + L)^{-1} \omega^{-1/2}.$$

The general form of the novel two-flavor pseudofermion action for domain-wall fermions with $H = c\gamma_5 D_w(1 + dD_w)^{-1}$ will be presented in a forthcoming paper [17].

Then, the partition function for the $SU(3)$ gauge theory with $N_f = 10$ massless optimal DWFs can be written as

$$Z' = \int [dU] \prod_{i=1}^{5} [d\phi^\dagger]_i [d\phi]_i$$

$$\times \exp\left(-S_g[U] - \sum_{i=1}^{5} \phi_i^\dagger K(0)^\dagger K(0) \phi_i\right). \quad (5)$$

We perform HMC simulations of all gauge ensembles with Eq. (5) on the five-dimensional lattice $L^4 \times 16$, for $L/a = \{8, 10, 12, 16, 20, 24, 32\}$. The boundary conditions of the gauge field are periodic in all directions, while the boundary conditions of the pseudofermion fields are antiperiodic in all directions. In the molecular dynamics, we use the Omelyan integrator [18] and the Sexton-Weingarten multiple-time scale method [19]. Moreover, we introduce an auxiliary heavy fermion field with mass $m_H a = 0.1$ ($m_q \ll m_H \ll m_{PV}$) similar to the case of the Wilson fermion [20]—the so-called mass preconditioning. The simulations are performed on GPU clusters with Nvidia GPUs (P100, GTX-1080Ti, GTX-1080, GTX-1070, GTX-1060, GTX-TITAN-X, GTX-TITAN-Z, and GTX-TITAN). Thermalization of each ensemble is performed on one computing node with 1–2 GPUs. Then, the thermalized configurations are distributed to 16–32 nodes for independent HMC simulations in multiple streams. For each gauge ensemble, we generate 4000–20 000 trajectories after thermalization, and sample one configuration every five trajectories, which yields 800–4000 configurations for measurements.

The chiral symmetry breaking due to finite $N_s = 16$ can be measured in terms of the residual mass of the massless fermion [21],

$$m_{res} = \frac{\langle \text{tr}(D_c^{-1})_{0,0} \rangle_U}{\langle \text{tr}[\gamma_5 D_c \gamma_5 D_c]_{0,0}^{-1} \rangle_U},$$

where D_c^{-1} denotes the massless fermion propagator, "tr" denotes the trace running over the color and Dirac indices, and the brackets $\langle \cdots \rangle_U$ denote averaging over all configurations of the gauge ensemble. The residual masses of all gauge ensembles in this work are summarized in Table I.

We observe that the variation of the residual mass is quite mild, ranging from $\sim 4.4 \times 10^{-5}$ to $\sim 8.5 \times 10^{-5}$, i.e., less than a factor of 2. Moreover, the residual mass of any lattice size L^4 is much smaller than the energy scale $\mu \simeq (cL)^{-1}$ of the finite-volume gradient flow scheme with $c = 0.3$,

$$(m_{res} a)_L \ll \mu a \simeq \frac{1}{c(L/a)}.$$

Even for the smallest μ of the largest lattice 32^4 in this work, the residual mass of any gauge ensemble satisfies

$$m_{res} a \ll \frac{1}{0.3 \times 32} \simeq 0.104.$$

Thus the effect of the residual masses on the renormalized couplings should be negligible for our analysis.

III. RENORMALIZED COUPLING OF THE FINITE-VOLUME GRADIENT FLOW SCHEME

To obtain the renormalized coupling of gauge theory on a finite lattice with volume L^4, we use the finite-volume gradient flow scheme [22], which is based on the idea of continuous smearing [23] or equivalently the gradient flow [24] to evaluate the expectation value $t^2 \langle E \rangle$, where E is the energy density of the gauge field and t is the flow time. This amounts to solving the discretized form of the following equation:

$$\frac{dB_\mu}{dt} = D_\nu G_{\nu\mu},$$

with the initial condition $B_\mu|_{t=0} = A_\mu$, where $G_{\nu\mu} = \partial_\nu B_\mu - \partial_\mu B_\nu + [B_\nu, B_\mu]$ and $D_\nu G_{\nu\mu} = \partial_\nu G_{\nu\mu} + [B_\nu, G_{\nu\mu}]$. As shown in Ref. [24], the gradient flow is a process of averaging a gauge field over a spherical region of root-mean-square radius $R_{rms} = \sqrt{8t}$. Moreover, since $t^2 \langle E \rangle$ is proportional to the renormalized coupling, one can use $c = \sqrt{8t}/L$ as a constant to define a renormalization scheme on a finite lattice, and obtain

$$g^2(L, a) = \frac{16\pi^2}{3[1 + \delta(c, a/L)]} \langle t^2 E(t) \rangle, \quad E(t) = \frac{1}{2} F_{\mu\nu} F_{\mu\nu}(t),$$
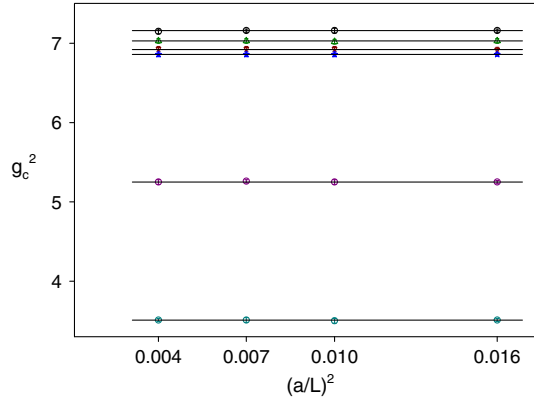
$$(6)$$

FIG. 1.   Tuning $g^2(L, a)$ on four primary lattices $L/a = \{8, 10, 12, 16\}$, for six targeted values of g_c^2. Each horizontal line is a constant fit. The fitted values are $g_c^2 = \{3.51(2), 5.25(2), 6.86(2), 6.92(3), 7.03(2), 7.16(2)\}$.

where a is the lattice spacing depending on the bare coupling g_0, E is the energy density, and the numerical factor on the rhs of Eq. (6) is fixed such that $g_c^2(L, a) = g_{\overline{\rm MS}}^2$ to the leading order. Here the coefficient $\delta(c, a/L)$ includes the tree-level finite-volume and finite-lattice-spacing corrections [25]. In this paper, we use the Wilson flow, the Wilson action, and the clover observable—the so-called WWC scheme—which is known to have very small tree-level cutoff effects [25]. Moreover, we fix $c = \sqrt{8t}/L = 0.30$.

For each targeted value of g_c^2, the renormalized couplings $g^2(L, a)$ of four primary lattices ($L/a = \{8, 10, 12, 16\}$) are tuned (in $6/g_0^2$) to the same g_c^2 with statistical error less than 0.5%. Here the statistical error is estimated using the jackknife method with a bin size of 10-15, of which the statistical error saturates. In Fig. 1, we plot the tuned renormalized coupling $g^2(L, a)$ versus $(a/L)^2$, for $L/a = \{8, 10, 12, 16\}$, and for six targeted values of g_c^2. Each horizontal line is a constant fit. The fitted values are $g_c^2 = \{3.51(2), 5.25(2), 6.86(2), 6.92(3)7.03(2), 7.16(2)\}$, with $\chi^2/{\rm d.o.f.} = \{0.19, 0.29, 0.14, 0.33, 0.19, 0.18\}$, respectively.

After the value of $6/g_0^2$ is determined for a chosen $g_c^2 = g^2(L, a)$, the simulation on the scaled ($s = 2$) lattice is performed at the same $6/g_0^2$ to obtain the renormalized coupling $g^2(sL, a)$. All renormalized couplings of $g^2(L, a)$ and $g^2(sL, a)$ are summarized in Table II. Each row gives the values of $g^2(L, a)$ and $g^2(sL, a)$ at the same $6/g_0^2$. Every four rows are grouped for the same targeted value of g_c^2.

IV. THE STEP-SCALING β FUNCTION $\beta(s, a/L, g_c^2)$ AND ITS CONTINUUM LIMIT

For each targeted value of $g_c^2 = g^2(L, a)$, we compute the step-scaling β function according to Eq. (1) for all lattice pairs $(sL, L)/a$ with fixed $s = 2$. Taking the

continuum limit $(a/L \to 0)$, $\beta(s, a/L, g^2)$ becomes $\beta(s, g^2)$,

$$\lim_{a/L \to 0} \beta(s, a/L, g^2) \equiv \beta(s, g^2) = \frac{g^2(sL) - g^2(L)}{\ln(s^2)}. \quad (7)$$

Moreover, if $\beta(s, g_c^2)$ is determined for several values of s, then it can be extrapolated to $s = 1$,

$$\lim_{s \to 1} \beta(s, g^2) = \beta(g^2) = \frac{dg^2(L)}{d \ln L^2} = -\frac{dg^2(\mu)}{d \ln \mu^2} = -\beta(g^2(\mu)), \quad (8)$$

where $\beta(g^2(\mu))$ is equal to the continuum β function in the momentum space. To fix our notation, we recall the β function to two-loop order in the $SU(3)$ gauge theory with N_f massless fermions in the fundamental representation,

$$\beta(g^2(\mu)) = \frac{dg^2}{d \ln \mu^2} = -\frac{b_1}{(4\pi)^2} g^4 - \frac{b_2}{(4\pi)^4} g^6 + O(g^8),$$

where $b_1 = 11 - 2N_f/3$ and $b_2 = 102 - 38N_f/3$.

If $\beta(g^2)$ has an IRFP, then $\beta(s, g^2)$ also has a corresponding IRFP, and vice versa. In this paper, we determine $\beta(2, g^2)$ of the $SU(3)$ lattice gauge theory with $N_f = 10$ massless optimal domain-wall fermions in the fundamental representation, using four lattice pairs $(2L, L)/a = \{(16, 8), (20, 10), (24, 12), (32, 16)\}$ for extrapolation to the continuum limit.

In Fig. 2, $\beta(s, a/L, g_c^2)$ is plotted versus $(a/L)^2$, for six targeted values of g_c^2. For each targeted g_c^2, the extrapolation to the continuum limit $(a/L \to 0)$ is performed with the linear fit $[A + B(a/L)^2]$ and the quadratic fit $[A + B(a/L)^2 + C(a/L)^4]$, respectively. Both fits give consistent results in the continuum limit, but the quadratic fits yield larger error bars. Note that for $g_c^2 = 7.16(2)$, the step-scaling β function for $(sL, L)/a = (16, 8)$ has large cutoff effects from $(a/L)^4$. Thus the linear fit only uses three data points from $(sL, L)/a = \{(20, 10), (24, 12), (32, 16)\}$. The results for $\beta(s, g_c^2)$ are summarized in Table III for both linear and quadratic fits. In the following, we compare the results in the second column of Table III with those of Ref. [2] and Ref. [6].

First, we check the value of $\beta(s, g_c^2) = 0.234(30)$ at $g_c^2 = 3.51(2)$, which is in good agreement with the value $0.23(1)$ obtained in Ref. [2]. This suggests that cubic-spline interpolation can work well in the regime where the renormalized coupling varies slowly with respect to the bare coupling $6/g_0^2$. In other words, the β function $\beta(s, g_c^2)$ reported in Ref. [2] should be valid for $0 \leq g_c^2 \leq 3.51$.

Next, we check the value of $\beta(s, g_c^2) = 0.318(45)$ at $g_c^2 = 5.25(2)$, which is quite smaller than the value $0.43(2)$ reported in Ref. [2]. This implies that cubic-spline interpolation fails in the regime where the renormalized
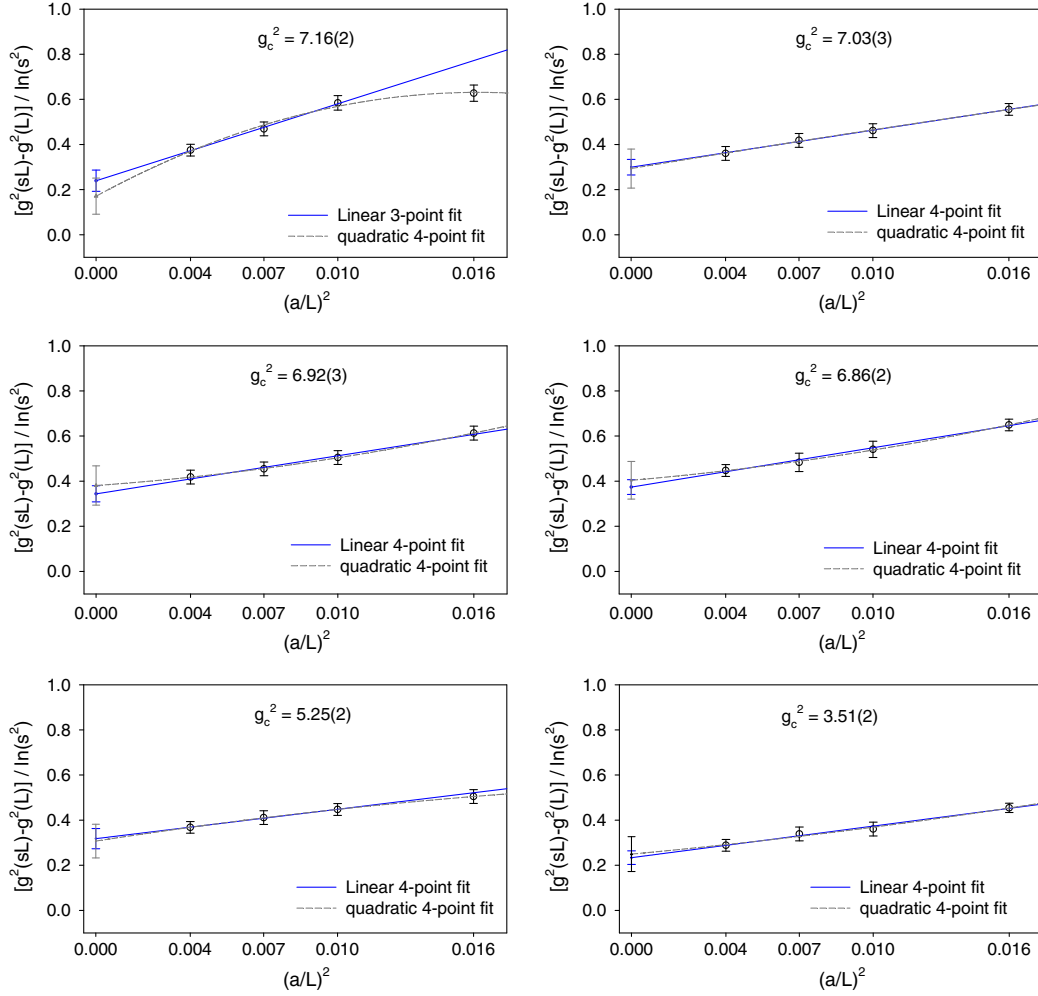
FIG. 2.   The step-scaling β functions of four lattice pairs $(sL, L)/a = \{(16,8), (20,10), (24,12), (32,16\}$ are plotted versus $(a/L)^2$, for $g_c^2 = \{7.16(2), 7.03(2), 6.92(3), 6.86(2), 5.25(2), 3.51(2)\}$. The extrapolation to the continuum limit is performed with the linear fit and the quadratic fit, respectively.

coupling varies rapidly with respect to the bare coupling $6/g_0^2$. Now the value of $\beta(s, g_c^2)$ at $g_c^2 = 5.25(2)$ is compatible with the result of a recent study of the $SU(3)$ gauge theory with $N_f = 10$ massless domain-wall fermions [6]. This suggests that the discrepancy between the results of Ref. [2] and Ref. [6] for $4.5 < g_c^2 < 6.0$ is likely due to the systematic error of interpolation.

The three data points at $g_c^2 = \{6.86(2), 6.92(3), 7.03(2)\}$, $\beta(s, g_c^2) = \{0.371(32), 0.344(36), 0.299(35)\}$, are quite larger than the corresponding ones $\{0.06(4), 0.02(5), 0.00(8)\}$ in Ref. [2]. This confirms that using interpolation would give unreliable results for $g^2(L, a)$ and $g^2(sL, a)$, especially in the regime where they vary rapidly with respect to the bare coupling $6/g_0^2$, and consequently yield an incorrect $\beta(s, a/L, g_c^2)$ as well as the extrapolated $\beta(s, g_c^2)$ in the continuum limit. Nevertheless, the resulting $\beta(s, g_c^2)$ seems to be able to capture some salient features of the β function, e.g., the increasing/decreasing trend of $\beta(s, g_c^2)$ with respect to g_c^2, even though it cannot give

the precise shape of the entire β function in the (g_c^2, β) plane.

Finally, we note that as g_c^2 is increased from 5.25(2) to 6.86(2), $\beta(s, g_c^2)$ increases from 0.318(45) to 0.371(32). This implies that the slope of $\beta(s, g_c^2)$ is positive for $g_c^2 \in [5.25, g_{max}^2]$, where $\beta(s, g_c^2)$ reaches the local maximum at g_{max}^2. Then for $g_c^2 > g_{max}^2$, the slope of $\beta(s, g_c^2)$ becomes negative, and $\beta(s, g_c^2)$ decreases to 0.371(32) at $g_c^2 = 6.86(2)$. To determine the exact location of g_{max}^2 as well as the precise shape of $\beta(s, g_c^2)$ in the vicinity g_{max}^2 is very challenging, since it requires many targeted values of g_c^2, and also we cannot rely on the renormalized couplings from interpolation, especially in this regime where the slope of $\beta(s, g_c^2)$ changes sign (from positive to negative).

V. EXTRAPOLATION OF $\beta(s, g^2)$

In Fig. 3, we plot $\beta(s, g_c^2)$ versus g_c^2 for $g_c^2 = \{6.86(2), 6.92(3), 7.03(2), 7.16(2)\}$. In Fig. 3(a) the data points are

obtained by continuum extrapolation with the linear fit, as listed in the second column of Table III, while in Fig. 3(b) the data points are obtained by continuum extrapolation with the quadratic fit, as listed in the fourth column of Table III. In both cases, the data points are well fitted by the linear approximation of $\beta(s, g^2)$,

$$\beta(s, g^2) = \left.\frac{d\beta(s, g^2)}{dg^2}\right|_{g_*^2} (g^2 - g_*^2) \equiv \beta_s^{(1)}(g^2 - g_*^2). \quad (9)$$

In Fig. 3(a) the linear fit gives

$$g_*^2 = 7.72 \pm 0.31, \quad (10)$$

$$\beta_s^{(1)} = 0.43 \pm 0.17, \quad (11)$$

with $\chi^2/\text{d.o.f.} = 0.06$, while in Fig. 3(b) the linear fit gives

$$g_*^2 = 7.38 \pm 0.18, \quad (12)$$

$$\beta_s^{(1)} = 0.81 \pm 0.36, \quad (13)$$

with $\chi^2/\text{d.o.f.} = 0.16$. Note that our convention for $\beta(s, g^2)$ in Eq. (7) is the negative of the conventional β function in the continuum (8) and thus gives a negative slope $\beta_s^{(1)}$ at the IRFP, as shown in Fig. 3. We omit the negative sign in Eqs. (11) and (13) to conform with the conventional β function in the continuum.

These two sets of results (10)–(13) are consistent with each other within error bars, which seems to imply the existence of an IRFP at $g_*^2 \in [7.20, 8.03]$. However, we have not measured $\beta(s, g_c^2)$ for $g_c^2 > 7.16$. Thus it is uncertain whether $\beta(s, g_c^2)$ would behave like Eq. (9) all the way from $g_c^2 = 7.16$ to g_*^2, or if it would start to bounce back at some point $g_{\min}^2 > 7.16$ and become an increasing function of g_c^2 for $g_c^2 > g_{\min}^2$. The former scenario implies

that the theory is infrared conformal with the fixed point at $g_*^2 \in [7.20, 8.03]$, while the latter suggests that the theory is near-conformal, depending on how closely $\beta(s, g_c^2)$ approaches zero.

VI. UNIVERSAL SCALING EXPONENT OF $\beta(g^2)$

In the former scenario, the coefficient $\beta_s^{(1)}$ can be used to determine the universal scaling exponent γ_g^* of the β function at the IRFP,

$$\beta(g^2) \simeq \frac{\gamma_g^*}{2}(g^2 - g_*^2), \quad (14)$$

with the relationship (see also Ref. [26])

$$\gamma_g^* = \frac{\ln\left(1 + \beta_s^{(1)}\ln(s^2)\right)}{\ln(s)}, \quad (15)$$

which can be obtained by integrating Eq. (8), and using Eqs. (14), (7), and (9):

$$\begin{aligned}
\ln(s^2) &= \int_L^{sL} d\ln(L^2) = \int_{g^2(L)}^{g^2(sL)} \frac{dg^2}{\beta(g^2)} \\
&\simeq \int_{g^2(L)}^{g^2(sL)} \frac{2dg^2}{\gamma_g^*(g^2 - g_*^2)} = \frac{2}{\gamma_g^*} \ln\left(\frac{g^2(sL) - g_*^2}{g^2(L) - g_*^2}\right) \\
&\simeq \frac{2}{\gamma_g^*} \ln\left(1 + \beta_s^{(1)}\ln(s^2)\right),
\end{aligned}$$

where

$$\begin{aligned}
g^2(sL) &= \beta(s, g^2)\ln(s^2) + g^2(L) \\
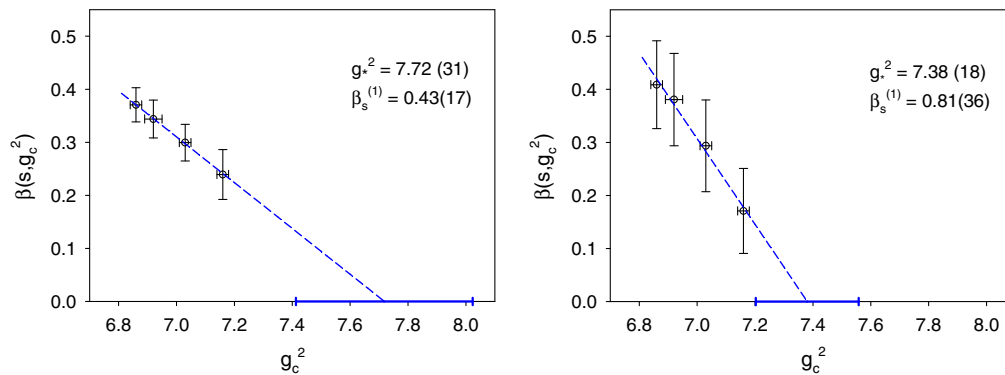&\simeq \beta_s^{(1)}(g^2(L) - g_*^2)\ln(s^2) + g^2(L)
\end{aligned}$$

has been used.

FIG. 3. Extrapolation of $\beta(s, g_c^2)$ with the linear fit using four data points close to the "fitted IRFP" g_*^2. (a) Four data points obtained by continuum extrapolation with the linear fit are used (as listed in the second column of Table III). (b) Four data points obtained by continuum extrapolation with the quadratic fit are used (as listed in the fourth column of Table III).

Note that in the limit $s \to 1$, Eq. (15) gives

$$\gamma_g^* = 2\beta_{s=1}^{(1)}. \tag{16}$$

The significance of Eqs. (15) and (16) is that the slope of $\beta(s, g^2)$ at the IRFP (with $s \neq 1$) can be used to determine that at $s = 1$, i.e., the slope of the β function $\beta(g^2)$ at the IRFP, which is equal to $\gamma_g^*/2$.

Substituting Eq. (11) into Eq. (15) gives

$$\gamma_g^* = 0.68 \pm 0.22, \tag{17}$$

while putting Eq. (13) into Eq. (15) gives

$$\gamma_g^* = 1.08 \pm 0.34. \tag{18}$$

These two results are consistent with each other within error bars. They are also compatible with the results in the weak-coupling perturbative theory—0.473 (the scheme-independent value to the fifth-order) and 0.853 (to four-loop order in the $\overline{\text{MS}}$ scheme)—as given in Ref. [27].

It is interesting to note that even though the interpolated $g^2(L, a)$ and $g^2(sL, a)$ in Refs. [1,2] cannot give a reliable determination of the β function $\beta(s, g_c^2)$, especially in the regime where $g^2(L, a)$ and $g^2(sL, a)$ vary rapidly with respect to $6/g_0^2$, they can still capture the slope of the β function (at the IRFP). Using the four data points $\beta(s, g_c^2) = \{0.154(44), 0.097(36), 0.037(49), -0.007(0.078)\}$ obtained in Ref. [2] at $g_c^2 = \{6.70(2), 6.80(2), 6.90(2), 7.00(2)\}$, respectively, the linear fit (see Fig. 4) gives $g_*^2 = 6.99(9)$ and the slope of the β function $\beta_s^{(1)} = 0.53(25)$, which in turn gives $\gamma_g^* = 0.80(30)$, which is in good agreement with Eqs. (17) and (18).
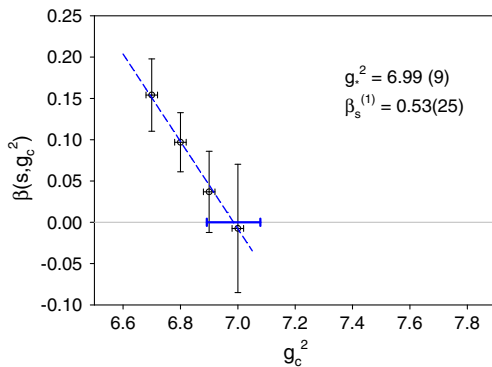

FIG. 4. Extrapolation of $\beta(s, g_c^2)$ with the linear fit, using four data points of $\beta(s, g_c^2)$ obtained in Ref. [2], with $g^2(L, a)$ and $g^2(sL, a)$ obtained by the cubic-spline interpolation.

VII. DISCUSSION AND CONCLUSION

In this paper we performed an improved study of the β function of $SU(3)$ gauge theory with $N_f = 10$ massless optimal domain-wall fermions in the fundamental representation. In the finite-volume gradient flow scheme with $c = \sqrt{8t}/L = 0.3$, the renormalized couplings $g^2(L, a)$ of four primary lattices ($L/a = \{8, 10, 12, 16\}$) were tuned (in $6/g_0^2$) to the same g_c^2 with a statistical error less than 0.5%. Then, the renormalized couplings $g^2(sL, a)$ of the scaled lattices ($sL/a = \{16, 20, 24, 32\}$ with $s = 2$) were computed at the same $6/g_0^2$ of the corresponding primary lattices. Using four lattice pairs $(sL, L)/a = \{(16, 8), (20, 10), (24, 12), (32, 16)\}$, the step-scaling β function $\beta(a, s/L, g_c^2)$ was computed and extrapolated to the continuum limit $\beta(s, g_c^2)$ (as summarized in Table III) for six targeted values of g_c^2. Based on the four data points of $\beta(s, g_c^2)$ at $g_c^2 = \{6.86(2), 6.92(3), 7.03(2), 7.16(2)\}$ (see Fig. 3), two different scenarios for this theory could emerge.

In the first scenario, $\beta(s, g_c^2)$ would behave like Eq. (9) all the way from $g_c^2 = 7.16$ to g_*^2, and the theory is infrared conformal. Combining the fitting results from Figs. 3(a) and 3(b) gives $g_*^2 = 7.55 \pm 0.36$, and the universal scaling exponent of $\beta(g^2)$, $\gamma_g^* = 0.88 \pm 0.40$.

In the second scenario, $\beta(s, g_c^2)$ would behave like a decreasing function of g_c^2 for $g_c^2 > 7.16$ until it reaches the local minimum at $g_{\min}^2$, when it bounces back and becomes an increasing function of g_c^2 for $g_c^2 > g_{\min}^2$. The question is how closely the minimum $\beta(s, g_{\min}^2)$ approaches zero.

To investigate whether the theory is near-conformal or conformal for $g_c^2 > 7.16$ would require much more computing resources than was available for this study. Note that the HMC simulations become more expensive as g_c^2 becomes larger (or, equivalently, $6/g_0^2$ becomes smaller).

Recently, a study of the β function in the $SU(3)$ lattice gauge theory with $N_f = 10$ massless staggered fermions in the fundamental representation was presented in Ref. [7], with a preview in Ref. [28]. The continuum β function $\beta(s, g_c^2)$ in Ref. [7] is a monotonic increasing function of $g_c^2 \in [5.0, 7.7]$, in complete disagreement with the four data points of $\beta(s, g_c^2)$ in Fig. 3. Such a dramatic discrepancy looks rather striking.

In the following, we compare the results of Ref. [7] at $g_c^2 = 7.0$ with those in this study at $g_c^2 = 7.03(2)$. In Ref. [7], the step-scaling β function $\beta(s, a/L, g_c^2)$ was obtained with five lattice pairs $(sL, L)/a = \{(24, 12), (32, 16), (36, 18), (40, 20), (48, 24)\}$, which is a monotonic decreasing function of $(a/L)^2$, for $g_c^2 = 7.0$. This is completely different from the $\beta(s, a/L, g_c^2)$ in this paper, which is a monotonic increasing function of $(a/L)^2$, as shown in the top-right panel of Fig. 2 for $g_c^2 = 7.03(2)$. Consequently, the continuum β function in Ref. [7] became very large, $\beta(s, g_c^2) = 0.75(4)$ at $g_c^2 = 7.0$, which

is completely different from the $\beta(s, g_c^2) = 0.299(35)$ at $g_c^2 = 7.03(2)$ in this paper (see Table III). What would cause such a dramatic discrepancy between these two studies of the β function of $SU(3)$ lattice gauge theory with $N_f = 10$ massless lattice fermions?

First, could it be due to the residual mass at finite $N_s = 16$ in this study? As shown in Table I, the residual masses are all very tiny and quite uniform across all lattice sizes and couplings. Even if the residual mass has some additive correction to the renormalized coupling, say, $g^2(L, a) \to g^2(L, a) + \delta(m_{res}a)$, it would be canceled in the step-scaling β function $[g^2(sL, a) - g^2(L, a)]/\ln(s^2)$, since $(m_{res}a)_{sL} \sim (m_{res}a)_L$. Thus the residual mass has almost no effect on either the step-scaling function $\beta(s, a/L, g_c^2)$ or its value in the continuum limit. So we rule out the possibility that the residual mass could change the slope of the step-scaling function $\beta(s, a/L, g_c^2)$ at $g_c^2 = 7.03(2)$ (see the top-right panel of Fig. 2) from positive to negative. Next, does the residual mass have any effect on the shape/location of the continuum β function in the (g_c^2, β) plane? Now, for g_c^2 itself, $g_c^2 \to g_c^2 + \delta(m_{res}a)$ without cancellation. Since $(m_{res}a)_L$ is almost constant (with fluctuations less than 20%), for all g_c^2 on the primary lattices ($L/a = 8$, 10, 12, 16) it gives $\delta(m_{res}a) \sim \delta$ for all g_c^2, and the curve of $\beta(s, g_c^2)$ in the (g_c^2, β) plane is shifted to $\beta(s, g_c^2 + \delta)$ with almost no change in its shape. If the theory is infrared conformal, the IRFP is shifted from g_*^2 to $g_*^2 + \delta$, while the slope $\beta_s^{(1)}$ of $\beta(s, g_c^2)$ at the IRFP and γ_g^* are not affected. In view of the tiny residual masses in Table I, we suspect that δ is already much smaller than the error of g_c^2 resulting from tuning $g^2(L, a) = g_c^2$ for all primary lattices. In general, for any study with DWFs, if $\delta(m_{res}a)$ is a monotonically increasing function of $g^2(L, a)$, then the shape of the curve $\beta(s, g_c^2)$ would be a little bit stretched along the positive direction of the g_c^2 axis, due to the nonuniformity of $\delta(m_{res}a)$. If the theory is infrared conformal, the measured location of the IRFP would be a little larger than the exact g_*^2 (at zero residual mass), and also the measured slope of the β function at the IRFP would be smaller than its exact $\beta_s^{(1)}$. Consequently, the measured universal scaling exponent would be a little smaller than the exact γ_g^* (at zero residual mass). Likewise, if the theory is infrared near-conformal, the measured g_{min}^2 would be a little larger than the exact g_{min}^2 (at zero residual mass). From the above discussions, the effect of the residual mass in this study should be very small. Thus it is impossible to change the slope/curvature of $\beta(s, g_c^2)$ in Fig. 3 from negative to positive. So we rule out the possibility that the residual mass could produce such a dramatic discrepancy in $\beta(s, g_c^2)$ at $g_c^2 \sim 7.0$, namely, 0.299(35) in Table III versus 0.75(4) in Ref. [7].

Next, could this be due to the volumes being too small in this study? Would it be possible to make a dramatic change

in the continuum extrapolation if we include a larger volume, say, 48^4 in our analysis? From the data for $\beta(s, a/L, g_c^2)$ at $g_c^2 = 7.03(2)$, as shown in the top-right panel of Fig. 2, the rate of change of $\beta(s, a/L, g_c^2)$ with respect to $(a/L)^2$ is rather small at any $(a/L)^2$. Even if we add a larger volume, say 48^4, with an additional data point of $\beta(s, a/L, g_c^2)$ at $(a/L)^2 = (1/24)^2 \sim 0.00174$, it is very unlikely that the slope of $\beta(s, a/L, g_c^2)$ would undergo a dramatic change from a small positive slope to a large negative slope in the limit $(a/L) \to 0$. Note that the $(a/L)^4$ correction gets smaller for larger L as $(a/L) \to 0$. Consequently, the deviation of the step-scaling β function $\beta(s, a/L, g_c^2)$ from the linear function of $(a/L)^2$ gets smaller as L gets larger. In other words, in this study adding an extra data point with a larger volume for the step-scaling function $\beta(s, a/L, g_c^2)$ at $g_c^2 = 7.03(2)$ is very unlikely to make a dramatic change to its value in the continuum limit $(a/L \to 0)$. Note that in this study only one data point of $\beta(s, a/L, g_c^2)$ at the largest $g_c^2 = 7.16(2)$ and at the smallest volume $(a/L)^2 = (1/8)^2 \sim 0.016$ has a noticeable correction from the $(a/L)^4$ term, as shown in the top-left panel of Fig. 2. On the other hand, if we omit the data point of the largest volume $(a/L)^2 = (1/16)^2 \simeq 0.004$ in the top-right panel of Fig. 2 for $g_c^2 = 7.03(2)$, and perform the continuum extrapolation with the linear fit, we get $\beta(s, g_c^2) = 0.306(54)$ with $\chi^2/\text{d.o.f.} = 0.13$, which is in good agreement with the result 0.299(35) obtained with four lattice pairs, as given in Table III. Thus we rule out the possibility that adding data points of $\beta(s, a/L, g_c^2)$ with larger volumes in this study could produce such a dramatic difference in $\beta(s, g_c^2)$ at $g_c^2 \sim 7.0$, namely, ~ 0.3 in Table III versus ~ 0.75 in Ref. [7].

Finally, we compare the actions in this study with those in Ref. [7]. The gauge action in Ref. [7] is the tree-level improved Symanzik gauge action, which is different from the Wilson plaquette action in this study. However, we do not expect that different gauge actions would cause such dramatic differences in any observables. Then we come to the possibility that the dramatic discrepancies are due to two different lattice fermion actions. If both lattice fermion Dirac operators belong to the same universality class of the continuum Dirac operator, then they should produce consistent results in the continuum limit. Could the staggered fermion operator violate fermion universality in the vicinity of the IRFP? This conjecture has been addressed by the authors of Ref. [6]; however, it was refuted by the authors of Ref. [28]. A nonperturbative analytic proof seems to be required to settle the issue of whether the (rooted) staggered fermions belong to the same universality class of the continuum Dirac operator, especially in the vicinity of the IRFP. At the moment, the results of this study could not rule out those in Ref. [7], and vice versa. Moreover, we do not see any other (systematic/statistical) possibilities that can reconcile the dramatic discrepancies between these two

studies of the β function of the $SU(3)$ lattice gauge theory with $N_f = 10$ massless lattice fermions.

To conclude, based on the four data points of $\beta(s, g_c^2)$ as shown in Fig. 3, we infer that the theory is infrared conformal or near-conformal. This also implies that the $SU(3)$ gauge theory with $N_f = 12$ massless fermions in the fundamental representation is most likely infrared conformal with an IRFP $g_*^2 < 7.2$. This prediction is consistent with a recent study with $N_f = 12$ domain-wall fermions, which suggests that the theory is infrared conformal with an IRFP $g_*^2 \sim 6$ [29].

[1] T. W. Chiu, arXiv:1603.08854.
[2] T. W. Chiu, Proc. Sci. LATTICE2016 (**2017**) 228.
[3] C. Pica, Proc. Sci. LATTICE2016 (**2016**) 015.
[4] B. Svetitsky, EPJ Web Conf. **175**, 01017 (2018).
[5] O. Witzel, Proc. Sci. LATTICE2018 (**2019**) 006.
[6] A. Hasenfratz, C. Rebbi, and O. Witzel, arXiv:1710.11578.
[7] Z. Fodor, K. Holland, J. Kuti, D. Nogradi, and C. H. Wong, Proc. Sci. LATTICE2018 (**2019**) 199.
[8] D. B. Kaplan, Phys. Lett. B **288**, 342 (1992).
[9] H. Neuberger, Phys. Lett. B **417**, 141 (1998).
[10] S. Duane, A. D. Kennedy, B. J. Pendleton, and D. Roweth, Phys. Lett. B **195**, 216 (1987).
[11] Z. Fodor, S. D. Katz, and K. K. Szabo, J. High Energy Phys. 08 (2004) 003.
[12] T. DeGrand and S. Schaefer, J. High Energy Phys. 07 (2006) 020.
[13] T. W. Chiu, Phys. Rev. Lett. **90**, 071601 (2003).
[14] T. W. Chiu, Phys. Lett. B **744**, 95 (2015).
[15] T. W. Chiu (TWQCD Collaboration), J. Phys. Conf. Ser. **454**, 012044 (2013).
[16] Y. C. Chen and T. W. Chiu (TWQCD Collaboration), Phys. Lett. B **738**, 55 (2014).
[17] Y. C. Chen and T. W. Chiu (TWQCD Collaboration), New two-flavors pseudofermion action for Monte Carlo simulation of domain-wall fermion (to be published).
[18] I. P. Omelyan, I. M. Mryglod, and R. Folk, Phys. Rev. Lett. **86**, 898 (2001).
[19] J. C. Sexton and D. H. Weingarten, Nucl. Phys. **B380**, 665 (1992).
[20] M. Hasenbusch, Phys. Lett. B **519**, 177 (2001).
[21] Y. C. Chen and T. W. Chiu (TWQCD Collaboration), Phys. Rev. D **86**, 094508 (2012).
[22] Z. Fodor, K. Holland, J. Kuti, D. Nogradi, and C. H. Wong, J. High Energy Phys. 11 (2012) 007.
[23] R. Narayanan and H. Neuberger, J. High Energy Phys. 03 (2006) 064.
[24] M. Luscher, J. High Energy Phys. 08 (2010) 071; 03 (2014) 92.
[25] Z. Fodor, K. Holland, J. Kuti, S. Mondal, D. Nogradi, and C. H. Wong, J. High Energy Phys. 09 (2014) 018.
[26] A. Hasenfratz and D. Schaich, J. High Energy Phys. 02 (2018) 132.
[27] T. A. Ryttov and R. Shrock, Phys. Rev. D **95**, 105004 (2017).
[28] Z. Fodor, K. Holland, J. Kuti, D. Nogradi, and C. H. Wong, Phys. Lett. B **779**, 230 (2018).
[29] A. Hasenfratz, C. Rebbi, and O. Witzel, arXiv:1810.05176.